THE JOURNAL OF PHYSICAL CHEMISTRY LETTERS
A JOURNAL OF THE AMERICAN CHEMICAL SOCIETY

pubs.acs.org/JPCL Letter

Direct Observation of Increased Free Carrier Generation Owing to Reduced Exciton Binding Energies in Polymerized Small-Molecule Acceptors

Jinyuan Zhang, Jianxin Guan, Yaogang Zhang, Shucheng Qin, Qingye Zhu, Xiaolei Kong, Qing Ma, Xiaojun Li, Lei Meng, Yuanping Yi,* Junrong Zheng,* and Yongfang Li*

Cite This: *J. Phys. Chem. Lett.* 2022, 13, 8816−8824 Read Online

ACCESS | Metrics & More | Article Recommendations | Supporting Information

ABSTRACT: Energy loss caused by exciton binding energy (E_b) has become a key factor that restricts further advancement of organic solar cells (OSCs). Herein, we used transient mid-IR spectroscopy to study direct photogeneration of free charge carriers in small-molecule acceptors (SMAs) Y6 and IDIC as well as polymerized SMAs (PSMAs) PYFT and PZ1. We found that free carrier concentration is higher in PSMAs than in their corresponding SMAs, indicating reduced exciton E_b, which is then confirmed by ultraviolet photoelectron spectroscopy, low-energy inverse photoemission spectroscopy, and film absorption spectra measurements. The measured E_b values of PYFT and PZ1 are 0.24 and 0.37 eV, respectively, smaller than those of Y6 (0.32 eV) and IDIC (0.47 eV). This work not only provides a method to directly monitor the photogenerated free carriers in OSC materials but also demonstrates that polymerization is an effective strategy to reduce the E_b, which is crucial to decrease the energy losses in high-performance OSCs.

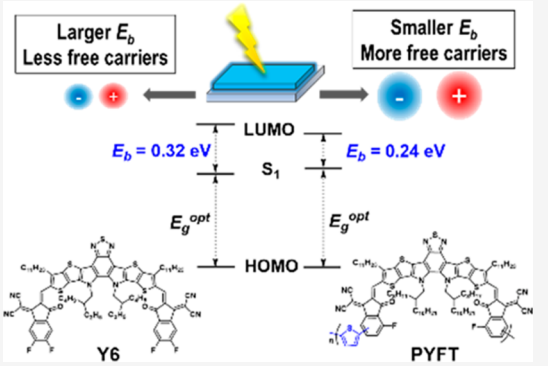

Both organic and inorganic semiconductors have been widely used in solar energy conversion as photovoltaic materials in solar cells. But the photophysical processes of these two types of materials are different,[1−5] mainly because the organic semiconductors have a much larger exciton binding energy (E_b), even by orders of magnitude, than the inorganic semiconductors.[6−11] E_b is defined as the energy difference between a bound electron−hole pair (exciton) and a free electron−hole pair.[12] In the solar cells based on inorganic semiconductors, Wannier-type excitons are usually formed upon illumination, which are able to spontaneously dissociate into free electrons and holes, benefitting from the small E_b that is usually smaller than the thermal energy k_BT at room temperature.[8,13] On the contrary, due to the substantially large E_b of organic semiconductors, tightly bound Frenkel-type excitons are predominantly generated in the organic solar cells (OSCs) upon photoexcitation, and they are difficult to separate into free charges to produce photocurrent.[14,15] Therefore, in actual OSC devices, two different organic semiconductor materials, featuring electron-donating (donor, D) and electron-accepting (acceptor, A) properties, were introduced in the active layer. They can form a heterojunction, and their energy-level difference at the interface serves as the driving force for charge transfer (CT) to overcome the exciton binding energies, generating free electrons (charge carriers) in the acceptor phase and holes (charge carriers) in the donor phase.[16−18] However, the introduction of this driving force inevitably leads to additional energy loss and lowers open-circuit voltage (V_{OC}) in the OSCs.[19−21] Although the power conversion efficiency (PCE) of the single-junction OSCs with the highest performance has exceeded 19%,[22] it still lags far behind the inorganic solar cells. Energy loss has been considered as a key factor that hindered the advancement of OSCs.[23,24] Therefore, organic photovoltaic (OPV) materials with smaller E_b are crucial for the future breakthrough of OSCs.[25−27]

At present, the rapid development of OSCs benefits from the emergence of high-performance narrow band gap small-molecule acceptors (SMAs). Especially the A-DA′D-A type of SMAs (such as Y6[28]) has brought OSCs into a new stage. This type of SMAs is known to realize high-performance OSCs even under a very small driving force, significantly reducing the energy losses.[29,30] This property might be attributed to the smaller exciton binding energies of these materials, derived from their rigid and planar framework as well as the intramolecular push−pull moieties.

Received: July 28, 2022
Accepted: September 12, 2022

https://doi.org/10.1021/acs.jpclett.2c02337
J. Phys. Chem. Lett. 2022, 13, 8816−8824

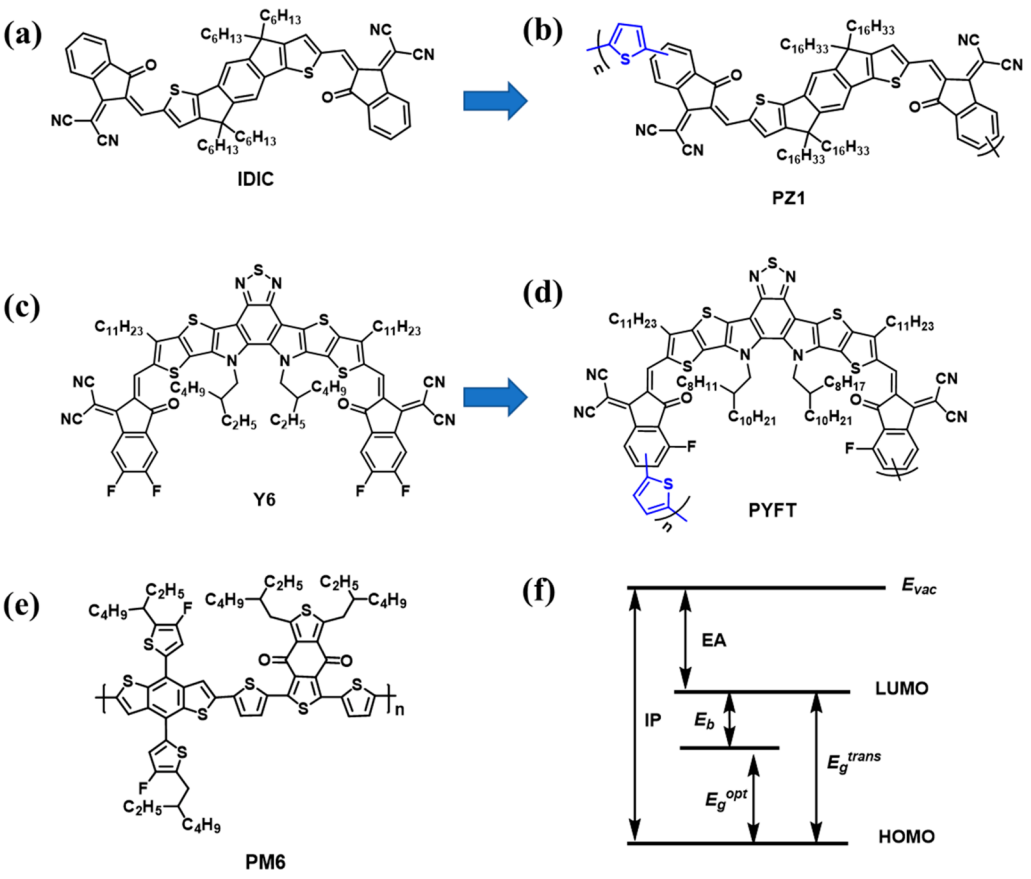

Figure 1. (a–e) Molecular structures of acceptors IDIC, PZ1, Y6, and PYFT and polymer donor PM6. (f) Schematic energy-level diagram that shows ionization potential (IP), electron affinity (EA), exciton binding energy (E_b), optical band gap (E_g^{opt}), and transport band gap (E_g^{trans}).

In 2017, Zhang et al. incorporated IDIC[31] as a building block and thiophene as a π-bridge linking unit to synthesize PZ1,[32,33] a polymerized small-molecule acceptor (PSMA), which preserves the advantages of IDIC such as strong absorption and narrow band gap while also showing the advantages of polymers such as good film formation and mechanical flexibility, etc. Using the same strategy, Y6-based PSMA and its derivatives, such as PY-T and PYFT, etc. were also synthesized, which increases the PCE of all-polymer solar cells (all-PSCs) to over 15%.[34−36] In polymers, generally speaking, the long main chains make it difficult to possess good crystallinity, while PSMA maintains good crystallinity and molecular packing, from which their molecular orbitals are highly overlapped, so that good intermolecular electron delocalization can be realized. At the same time, the elongated π conjugation promotes intrachain electron delocalization, leading to larger spatial separation of the holes and electrons. Both features could result in the reduction of the exciton binding energy.[27] Unfortunately, exciton binding energy cannot be directly measured, as it is defined as the difference between the transport band gap (E_g^{trans}) and optical band gap (E_g^{opt}): $E_b = E_g^{trans} - E_g^{opt}$, where E_g^{trans} and E_g^{opt} have to be measured separately.[6,38] As shown in Figure 1f, E_g^{trans} is the energy of free electron and hole, and E_g^{opt} refers to the energy of the lowest excited state of the semiconductor.

In this work, we studied the photophysical properties of four acceptors, including SMAs Y6 and IDIC, and their corresponding PSMAs PYFT and PZ1(Figures 1a–d) from the viewpoint of vibrational spectroscopy. We first performed the steady-state infrared (IR) absorption experiment and calculations of the four materials to get a basic idea of their vibrational modes in the ground state. And then we used femtosecond transient IR spectroscopy to get a better insight into their vibrations in the excited state. The transient species such as free carriers could be identified, and their lifetimes were extracted from the kinetic trace. Besides the two neat SMAs and two PSMAs, donor–acceptor blends of PM6:Y6 and PM6:PYFT (Figure 1e), which were commonly used in OSCs with high PCEs,[28,35] were chosen to study the free carrier generation via photoinduced charge transfer process in heterojunction active layers. Furthermore, in order to study the correlation between the relative yield of free carrier and exciton binding energy in each OPV material, we experimentally determined the E_b of these materials using E_g^{trans} calculated from ultraviolet photoelectron spectroscopy (UPS) and low-energy inverse photoemission spectroscopy (LEIPS), and E_g^{opt} measured from UV–vis absorption spectra. The results show that the PSMAs do possess smaller E_b than the corresponding SMAs, which demonstrates that polymerization is an effective approach to reduce the E_b of SMAs.

Fourier transform infrared spectroscopy (FTIR) was used to measure the ground-state vibrational absorption for the SMAs Y6 and IDIC and the PSMAs PYFT and PZ1. Gaussian was used to simulate the vibrational modes of the molecules. The measured and calculated full FTIR spectra were provided in Figure S1 in the Supporting Information.

The FTIR spectrum of Y6 exhibits characteristic peaks at 1230, 1290, 1340, and 1360 cm^{-1} for C–H rocking and scissoring modes, at 1427, 1505, and 1536 cm^{-1} for C=C and C=N stretching modes related to its fused aromatic core, at

https://doi.org/10.1021/acs.jpclett.2c02337
J. Phys. Chem. Lett. 2022, 13, 8816−8824

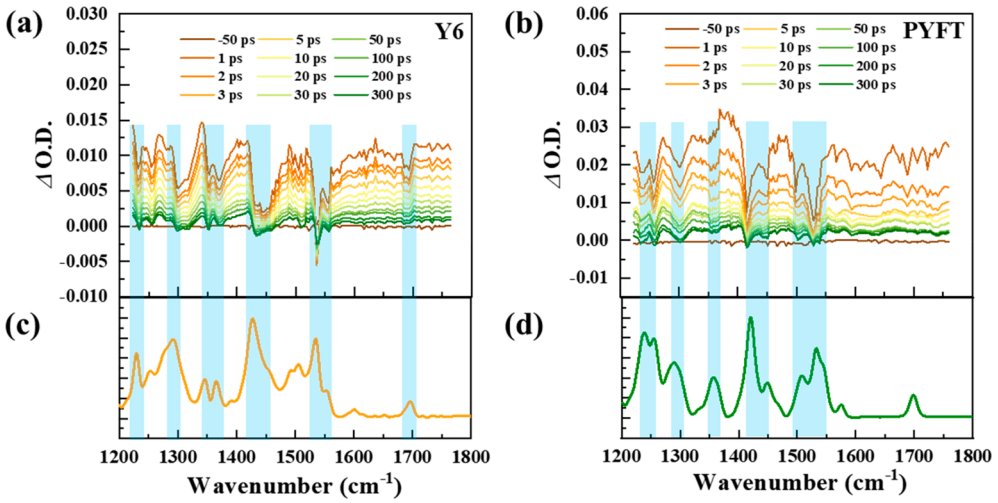

Figure 2. Transient IR spectra of (a) Y6 and (b) PYFT pristine films at selected delay times. FTIR spectra of (c) Y6 and (d) PYFT pristine films, enlarged in the range of 1200−1800 cm^{-1}, showing the matches with some GSB dips in the transient spectra.

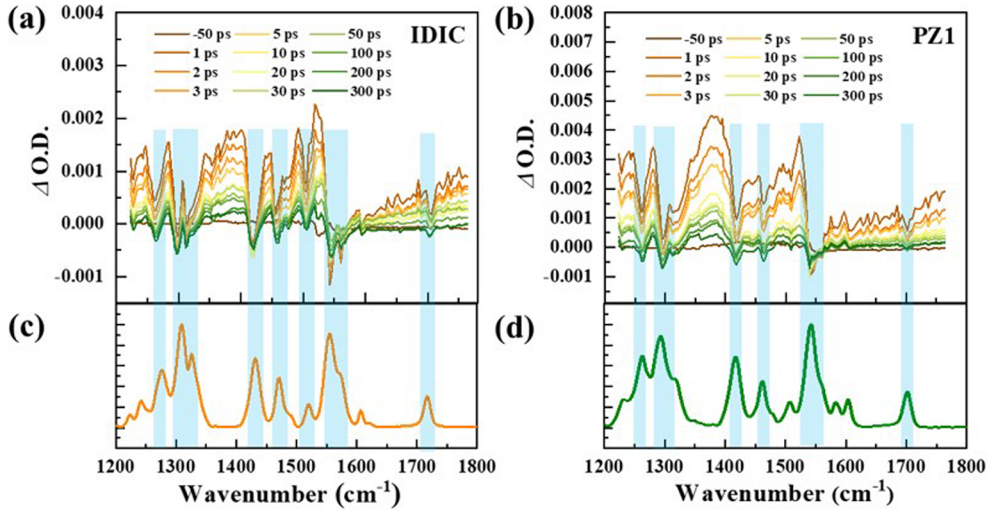

Figure 3. Transient IR spectra of (a) IDIC and (b) PZ1 pristine films at selected delay times. FTIR spectra of (c) IDIC and (d) PZ1 pristine films, enlarged in the range of 1200−1800 cm^{-1}, showing the matches with some GSB dips in the transient spectra.

1696 cm^{-1} for C═O stretching and a distinct peak at 2214 cm^{-1} for C≡N stretching on the ending group, and several C−H stretching modes of the side chains around 2900 cm^{-1}. For the acceptor IDIC, several C−H rocking modes are shown around 1300 cm^{-1}, three strong peaks of its aromatic core are found at 1411, 1452, and 1538 cm^{-1}, and C═O and C≡N stretching are at 1707 and 2222 cm^{-1}, respectively. No significant difference was found for the FTIR spectra of the PSMAs PYFT and PZ1, in comparison with their corresponding SMAs, since they have basically the same molecular backbone and functional groups as the SMAs. But it is obvious that the intensity of C−H stretching peaks from 2800 to 3000 cm^{-1} in the PSMAs is much stronger than those in the corresponding SMAs, because of the longer side chains in PSMAs.

Transient IR spectroscopy, combined with ultrahigh temporal and spectral resolution, is one of the most powerful tools to reveal intrinsic mechanisms of a series of photophysical and photochemical phenomena by capturing the structural evolution of molecules, different behavior of electron, and molecular motion. Transient IR spectroscopy has been widely used in various research fields such as reaction mechanism,[39,40] mechanism of molecular luminescence,[41,42] vibrational coupling,[43,44] kinetics and structure of proteins and peptides,[45−47] exciton behavior,[48−50] and charge and energy transfer.[51,52]

We used the visible pump/IR probe ultrafast spectroscopy to study the relaxation process of vibrational behavior of the organic semiconductor materials in their excited state. Upon 750 nm excitation, Y6 reaches its first locally excited state S1. As shown in Figure 2a, a broad band absorption appears, which originates from free carrier formation.[37,53−58] The ground-state bleach (GSB) of a series of vibrational modes attributed to conjugated skeleton vibrations and C═O stretching mode overlay on the broad band absorption of free carriers, matching the steady-state FTIR spectrum (Figure 2c) with slight frequency shifts induced by the electronic excitation. By investigating the vibrational behavior of the excited state, we can understand the distribution of free carriers on the excited state of the Y6 molecule, because some vibrational modes have stronger coupling to the electron transition dipole moment than others, resulting in deeper GSBs in the spectra.

https://doi.org/10.1021/acs.jpclett.2c02337
J. Phys. Chem. Lett. 2022, 13, 8816−8824

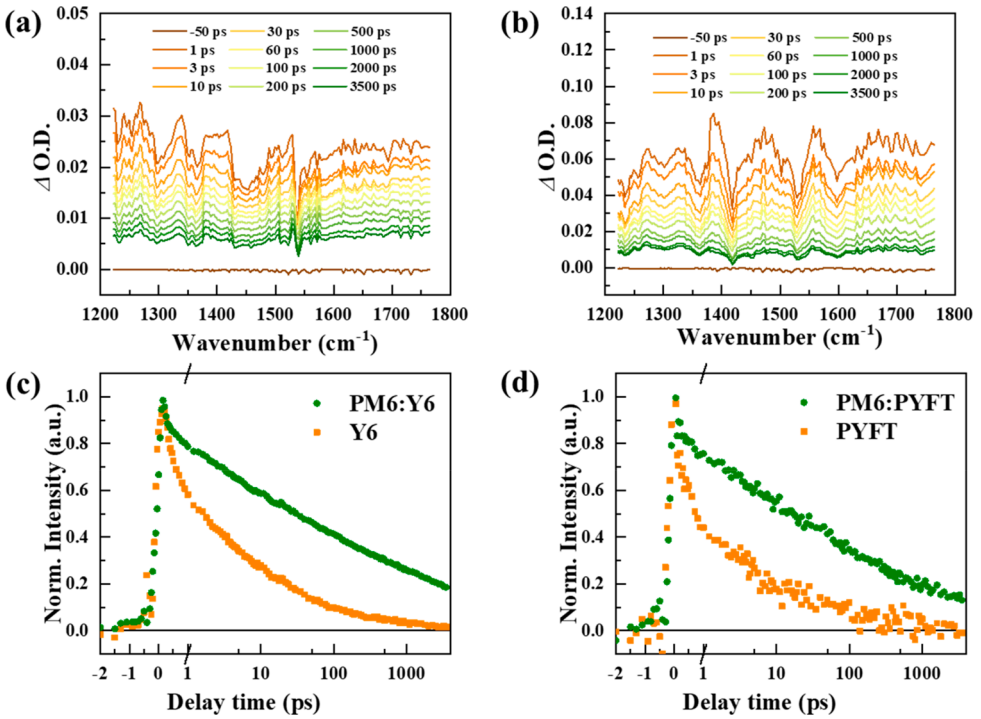

Figure 4. Transient IR spectra of (a) PM6:Y6 and (b) PM6:PYFT blend films at selected delay times. (c) Kinetic traces monitoring at 1400 cm^{-1} for PM6:Y6 (green) and Y6 (orange) films. (d) Kinetic traces monitoring at 1400 cm^{-1} for PM6:PYFT(green) and PYFT (orange) films.

The absorption signal reaches maxima almost instantaneously, within the instrument response function (IRF) of our experiments (~100 fs), indicating an ultrafast generation of free carriers in the film. The maximal intensity of the absorption signal allows us to approximately estimate the initial concentration of photogenerated free carriers, and the decay dynamics of this signal reflects the lifetime of the free carriers. Figure S2 in the Supporting Information displays the fitting of the kinetic traces from the spectrum, giving the lifetime of photogenerated free carriers of ~200 ps, much shorter than the lifetimes of inorganic semiconductors and the perovskite photovoltaic materials.[59]

As shown in Figure 2b, under the same film thickness, excitation fluence and similar extinction coefficient (see Figure S3 in Supporting Information), the absorption maxima of the polymer PYFT is around 0.03 OD, which is significantly stronger than that of the SMA Y6 (~0.015 OD), suggesting a higher concentration of photogenerated free carriers. This is possibly due to the smaller E_b of PYFT, which is more conducive to the dissociation of excitons into free electrons and holes. The result indicates that the polymerization of SMA can reduce their E_b values. In the transient IR spectra of PYFT, we also found that the GSB dips are generally less intense than that of Y6, implying that the coupling between electron and vibration transitions is reduced due to the polymerization. The GSBs at 1350 and 1700 cm^{-1}, corresponding to the bending mode of C−H on the vinyl and stretching mode of C═O on the ending group, respectively, show up in Y6 but are nearly absent in PYFT, which means the distribution of free charge carriers is different in the two molecules. Another GSB that is significantly weakened is at 1530 cm^{-1}, which corresponds to the stretching of the entire backbone of PYFT, especially the two C═C vinyl groups that connect to the ending groups. The attenuation of this vibration is mainly because the movement of the backbone is suppressed after polymerization, reducing its coupling to the electronic excited state.

We also performed transient IR experiments on a different pair of molecules, namely, SMA IDIC and PSMA PZ1. The spectra at selected time delays are shown in Figure 3, and the global fitting of the spectra are given in Figure S4 in the Supporting Information. The excitation wavelength was set at 650 nm, and the laser fluence was maintained the same as the previous experiments for Y6 and PYFT. Similarly, we observed that IDIC also produced a continuous absorption band of free carriers in the mid-IR region, with some dips of GSB presented in the spectra as well. When we tested the PSMA PZ1, which has the same building block of IDIC, we found PZ1 produced more photogenerated carriers (~0.004 OD, see Figure 3b) than IDIC (~0.002 OD, see Figure 3a). This provides another example that polymerization of SMA can reduce the exciton binding energy. The lifetimes of the free carriers for the two materials are similar, and both fitted to be around 100 ps. The weaker GSB intensity at 1530 cm^{-1} was observed in the PSMA PZ1 as well due to the same effect of weakened vibrational coupling of the polymer backbone.

We then investigated the free charge carrier properties in the donor/acceptor blend films. Compared to direct photogeneration, free charge carriers should be more efficiently yielded via CT reaction at the D/A interface in the heterojunction active layer.[16,17,60] Thus, heterojunction structure was always required for achieving high photocurrent in real OSCs. In order to probe the mechanism of free charge carrier generation in the active layers of high-performance OSCs, transient IR experiments were conducted on the blend films of PM6:Y6 and PM6:PYFT. The acceptors were selectively excited with pump wavelength at 750 nm to study the hole-transfer process. As shown in Figure 4a,b, the spectra showed distinct broad absorption of free charge carriers with some GSBs matching the FTIR of blend films (Figure S5 in

https://doi.org/10.1021/acs.jpclett.2c02337
J. Phys. Chem. Lett. 2022, 13, 8816−8824

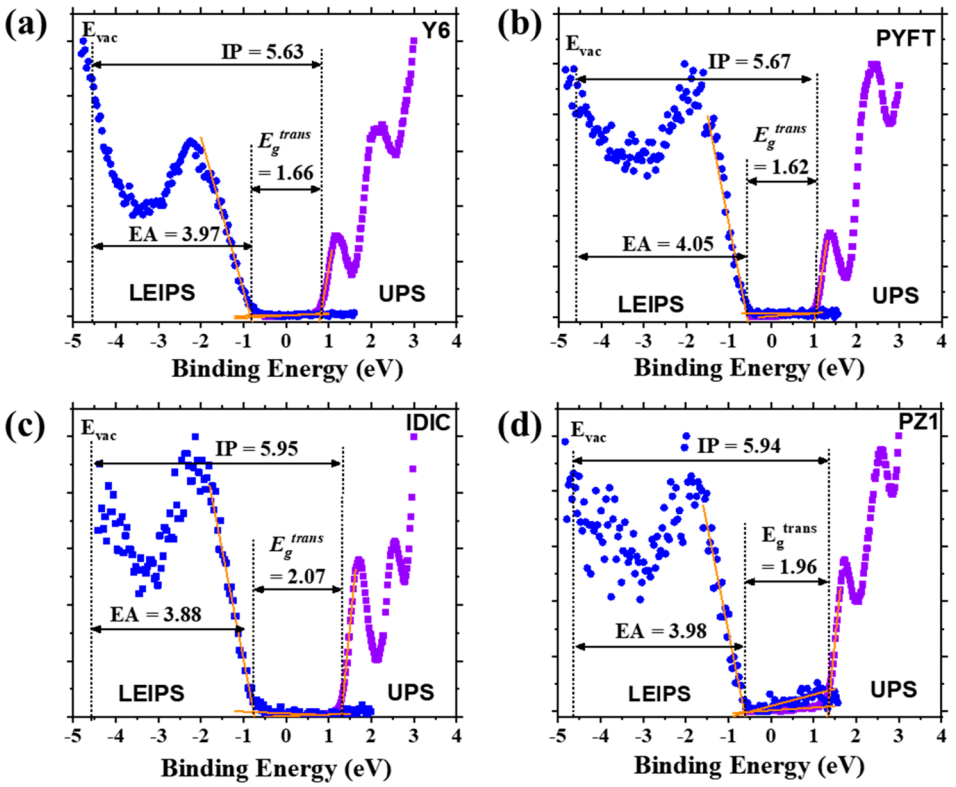

Figure 5. LEIPS and UPS spectra with linear extrapolation of (a) Y6, (b) PYFT, (c) IDIC, and (d) PZ1 showing IP, EA, and E_g^{trans} of the materials in solid film.

Supporting Information). The free charge carrier could originate from both mechanisms of charge photogeneration and CT. Therefore, a higher absorption intensity was observed in the transient IR spectra of both blend films compared to the single-component films. The increased yield of free charge carriers has benefited from the CT process that split the excitons into electrons and holes. Besides higher absorption intensity, the blend films also display much longer carrier lifetimes (5.2 ns for PM6:Y6 and 3.7 ns for PM6:PYFT, see Figure S6 in Supporting Information) compared to Y6 (218 ps) and PYFT (159 ps) neat films, which implies strongly inhibited charge recombination in the blend films. The prolonged lifetime is mainly attributed to stabilization of free charge carriers in the internal electric field created by the donor and acceptor. As a result, the higher free charge carrier concentration will boost the photocurrent in the device, and the much longer lifetime provides sufficient time for the free carriers to transport to the electrode. Therefore, the formation of D/A heterojunction is necessary in high-performance OSCs.

In order to elucidate the observation in the transient IR experiment, the exciton binding energies of Y6, IDIC and the PSMAs PYFT and PZ1 were determined experimentally.

First, the energy of transport gap E_g^{trans} is required to obtain E_b. Transport gap refers to the energy gap between the top of the valence band and the bottom of the conduction band, which is measured as the ionization potential (IP) and electron affinity (EA) of the material, respectively.[61] Thus, E_g^{trans} reflects the energy threshold for creating free electrons or holes in semiconductors. Ultraviolet photoelectron spectroscopy (UPS) and inverse photoemission spectroscopy (IPES) are reliable methods to measure the EA and IP for organic semiconductor films.[62] In this work, we use UPS to measure the IP of the four compounds, while we use low-energy inverse photoemission spectroscopy (LEIPS) instead IPES to measure EAs, because conventional IPES has a concern of damaging the target materials during the test, resulting in low resolution and bad reproducibility.[63] LEIPS uses low-energy electrons (<4 eV) that could reduce the damage to the material, which is more suitable for organic compounds. Samples of Y6, IDIC, PYFT, and PZ1 were prepared on indium tin oxide (ITO) glass substrates as thin films. The IP of each material was calculated based on IP = $E_{He-I} - \Delta E$, where ΔE is the kinetic energy difference between the high-energy edge cutoff and the low-energy onset of secondary electron emission, as shown in Figures S7 & S8 in the Supporting Information, and E_{He-I} = 21.22 eV, which is the photon energy of ultraviolet radiation source. As shown in Figure 5, Y6 and PYFT both showed IPs of around 5.6 eV, while IDIC and PZ1 showed larger IPs above 5.9 eV.

LEIPS measurements were performed on the same batch of samples as UPS in order to keep consistency of the data. The EA values were directly obtained from the LEIPS spectra as the energy difference between the emitted photon and the vacuum energy level (see Figures S9 in Supporting Information). It is obvious that both PSMAs PYFT (4.05 eV) and PZ1 (3.98 eV) exhibit larger EAs compared with their corresponding SMAs Y6 (3.97 eV) and IDIC (3.88 eV), respectively, suggesting that polymerization could bring down the energy of the lowest unoccupied molecular orbitals. For the absorption that we used to determine the E_g^{opt}, although PZ1 showed almost the same absorption spectrum as IDIC, PYFT exhibited blue-shifted absorption spectra after polymerization, corresponding to a larger E_g^{opt}, which further decreases the E_b. With the optical band gap E_g^{opt} values extracted from the absorption onset in the UV−vis spectrum (see Figure S10 in Supporting Information), we could calculate the exciton binding energy

https://doi.org/10.1021/acs.jpclett.2c02337
J. Phys. Chem. Lett. 2022, 13, 8816−8824

using the equation $E_b = E_g^{trans} - E_g^{opt}$. The measured IP and EA and calculated E_g^{trans}, E_g^{opt}, and E_b were summarized in Table 1. Apparently, the E_b values of the PSMAs polymer

Table 1. Physicochemical Property Data for Y6, PYFT, IDIC, and PZ1

compound	IP (eV)	EA (eV)	E_g^{trans} (eV)	λ_{onset} (nm)	E_g^{opt} (eV)	E_b (eV)
Y6	5.63	3.97	1.66	924	1.34	0.32
PYFT	5.67	4.05	1.62	897	1.38	0.24
IDIC	5.95	3.88	2.07	776	1.60	0.47
PZ1	5.94	3.98	1.96	780	1.59	0.37

PYFT (0.24 eV) and PZ1 (0.37 eV) are smaller than those of their corresponding SMAs Y6 (0.32 eV) and IDIC (0.47 eV), which means that the polymerization strategy efficiently reduces the energy barriers for the excitons to dissociate into free charges. It should be mentioned that, although the organic semiconductors possess the larger exciton binding energies, there are still an observable number of free charges upon photoexcitation as mentioned above. He et al. also reported direct charge generation in organic semiconductor zinc phthalocyanine with an exciton binding energy of over 0.28 eV.[58]

Among the reported photovoltaic parameters of OSCs, we notice that higher V_{oc} values were often obtained in the PSMA-based than the SMA-based devices, which indicates smaller energy losses (E_{loss}) in the PSMA-based OSCs. For example, the V_{oc} of the OSCs based on the Y-series SMAs are usually around 0.86 V,[28,64,65] while the V_{oc} of the OSCs based on the Y6-derived PSMAs are normally found to be 0.9 V and above.[35,66,67] The higher V_{oc} could be related to the lower E_b in PSMAs. Therefore, PSMA provides a feasible way to reduce E_{loss}, which is significant for achieving higher efficiency in OSCs in the future.

To further shed light on the effect of polymerization on the exciton binding energies of the SMAs, density functional theory (DFT) and time-dependent (TD) DFT calculations were conducted for the SMAs and the PSMAs.[68,69] The theoretical models for PSMAs considered in the present work and the details of theoretical calculation can be found in the Supporting Information. The calculated IP, EA, E_g^{trans}, E_g^{opt}, and E_b under consideration of the impact of surrounding dielectric medium are given in Table S2 in the Supporting Information together with hole delocalization index (HDI) and electron delocalization index (EDI). From Table S2 in the Supporting Information, it can be found that the polymerization mainly influences the E_b by decreasing IP but increases the EA of the SMA and eventually leads to a smaller E_g^{trans}, which is crucial for obtaining a lower E_b. And the calculated results of E_b for the SMAs Y6 and IDIC are in good agreement with the corresponding experimental values with only minor differences (0.02 eV for Y6 and 0.08 eV for IDIC). Although the theoretical E_b values of the PSMAs are not so satisfactory compared with experimental results, which may be caused by the combination of only two repeating unit models and a more complex polymer environment, it can still reflect the trend of decreasing E_b from SMAs to PSMAs. Comparing the HDI and EDI shown in Table S2 in the Supporting Information, we can also find that the HDIs and EDIs of PSMAs are smaller than those of SMAs by about 1.5, which suggests that the polymerization results in the stronger hole/electron delocalization. This phenomenon can be understood more intuitively in the real space representation of hole and electron distributions, as shown in Figure S11 in the Supporting Information. The enhancement of hole/electron delocalization of PSMAs does contribute to weaken the electron−hole Coulomb attraction and eventually leads to smaller exciton binding energies.

In conclusion, we observed direct photogeneration of free carriers in organic semiconductor solid films of Y6, IDIC, PYFT, and PZ1 using transient mid-IR spectroscopy. By investigating the vibrational behavior in the excited state, we can understand the distribution of free carriers on the excited state of the molecules. The free carrier concentration is higher in the PSMAs PYFT and PZ1 compared to their corresponding SMAs Y6 and IDIC due to their reduced exciton binding energies. The lifetimes of photogenerated free carriers of the organic semiconductors are on the order of hundreds of picoseconds, much shorter than that of the inorganic semiconductors. After a D/A heterojunction is formed, PM6:Y6 and PM6:PYFT blend films display much higher free carrier concentration as well as longer lifetime of over 3 ns because of CT reactions. The reduction of exciton binding energies in PSMAs are demonstrated by the measurements of UPS, LEIPS, and absorption spectra. The E_b of PSMAs PYFT and PZ1 are found to be 0.24 and 0.37 eV, respectively, which is significantly reduced compared to 0.32 and 0.47 eV for the SMAs Y6 and IDIC. DFT calculation illustrates that the reduction of E_b in PSMAs stems from the weakened Coulomb interaction, which is caused by the enhancement of hole/electron delocalization upon polymerization. Our results demonstrate that polymerization is an effective approach to reduce the E_b of SMAs, which is crucial to improve the energy losses to achieve high-performance OSCs.

■ ASSOCIATED CONTENT

Supporting Information

The Supporting Information is available free of charge at https://pubs.acs.org/doi/10.1021/acs.jpclett.2c02337.

Instrumental and calculation details as well as spectra of FTIR, transient IR, UV−vis, UPS, and LEIPS (PDF)

■ AUTHOR INFORMATION

Corresponding Authors

Yuanping Yi − *Beijing National Laboratory for Molecular Sciences, CAS Key Laboratory of Organic Solids, Institute of Chemistry, Chinese Academy of Sciences, Beijing 100190, China; School of Chemical Science, University of Chinese Academy of Sciences, Beijing 100049, China;* orcid.org/0000-0002-0052-9364; Email: ypyi@iccas.ac.cn

Junrong Zheng − *College of Chemistry and Molecular Engineering, Peking University, Beijing 100871, China;* orcid.org/0000-0002-4472-8576; Email: junrong@pku.edu.cn

Yongfang Li − *Beijing National Laboratory for Molecular Sciences, CAS Key Laboratory of Organic Solids, Institute of Chemistry, Chinese Academy of Sciences, Beijing 100190, China; School of Chemical Science, University of Chinese Academy of Sciences, Beijing 100049, China; Laboratory of Advanced Optoelectronic Materials, Suzhou Key Laboratory of Novel Semiconductor Materials and Devices, College of Chemistry, Chemical Engineering and Materials Science, Soochow University, Suzhou 215123 Jiangsu, China;*

https://doi.org/10.1021/acs.jpclett.2c02337
J. Phys. Chem. Lett. 2022, 13, 8816−8824

orcid.org/0000-0002-2565-2748; Email: liyf@iccas.ac.cn

Authors

Jinyuan Zhang − *Beijing National Laboratory for Molecular Sciences, CAS Key Laboratory of Organic Solids, Institute of Chemistry, Chinese Academy of Sciences, Beijing 100190, China*

Jianxin Guan − *College of Chemistry and Molecular Engineering, Peking University, Beijing 100871, China*

Yaogang Zhang − *Beijing National Laboratory for Molecular Sciences, CAS Key Laboratory of Organic Solids, Institute of Chemistry, Chinese Academy of Sciences, Beijing 100190, China; School of Chemical Science, University of Chinese Academy of Sciences, Beijing 100049, China*

Shucheng Qin − *Beijing National Laboratory for Molecular Sciences, CAS Key Laboratory of Organic Solids, Institute of Chemistry, Chinese Academy of Sciences, Beijing 100190, China; School of Chemical Science, University of Chinese Academy of Sciences, Beijing 100049, China*

Qingye Zhu − *College of Chemistry and Molecular Engineering, Peking University, Beijing 100871, China*

Xiaolei Kong − *Beijing National Laboratory for Molecular Sciences, CAS Key Laboratory of Organic Solids, Institute of Chemistry, Chinese Academy of Sciences, Beijing 100190, China; School of Chemical Science, University of Chinese Academy of Sciences, Beijing 100049, China*

Qing Ma − *Beijing National Laboratory for Molecular Sciences, CAS Key Laboratory of Organic Solids, Institute of Chemistry, Chinese Academy of Sciences, Beijing 100190, China; School of Chemical Science, University of Chinese Academy of Sciences, Beijing 100049, China*

Xiaojun Li − *Beijing National Laboratory for Molecular Sciences, CAS Key Laboratory of Organic Solids, Institute of Chemistry, Chinese Academy of Sciences, Beijing 100190, China*

Lei Meng − *Beijing National Laboratory for Molecular Sciences, CAS Key Laboratory of Organic Solids, Institute of Chemistry, Chinese Academy of Sciences, Beijing 100190, China; School of Chemical Science, University of Chinese Academy of Sciences, Beijing 100049, China;* orcid.org/0000-0003-2775-362X

Complete contact information is available at: https://pubs.acs.org/10.1021/acs.jpclett.2c02337

Notes

The authors declare no competing financial interest.

■ ACKNOWLEDGMENTS

This work was supported by National Key Research and Development Program of China (Nos. 2019YFA0705900 and 2017YFA0204702) funded by MOST, the National Natural Science Foundation of China (Nos. 52103243, 51820105003, 61904181, 52173188, 21927901, and 22173108), and the Basic and Applied Basic Research Major Program of Guangdong Province (No. 2019B030302007).

■ REFERENCES

(1) Clarke, T. M.; Durrant, J. R. Charge Photogeneration in Organic Solar Cells. *Chem. Rev.* **2010**, *110*, 6736−6767.

(2) Falke, S. M.; Rozzi, C. A.; Brida, D.; Maiuri, M.; Amato, M.; Sommer, E.; De Sio, A.; Rubio, A.; Cerullo, G.; Molinari, E.; Lienau, C. Coherent Ultrafast Charge Transfer in An Organic Photovoltaic Blend. *Science* **2014**, *344*, 1001−1005.

(3) Gelinas, S.; Rao, A.; Kumar, A.; Smith, S. L.; Chin, A. W.; Clark, J.; van der Poll, T. S.; Bazan, G. C.; Friend, R. H. Ultrafast Long-range Charge Separation in Organic Semiconductor Photovoltaic Diodes. *Science* **2014**, *343*, 512−516.

(4) Stoltzfus, D. M.; Donaghey, J. E.; Armin, A.; Shaw, P. E.; Burn, P. L.; Meredith, P. Charge Generation Pathways in Organic Solar Cells: Assessing the Contribution from the Electron Acceptor. *Chem. Rev.* **2016**, *116*, 12920−12955.

(5) Marinova, N.; Valero, S.; Delgado, J. L. Organic And Perovskite Solar Cells: Working Principles, Materials And Interfaces. *J. Colloid Interface Sci.* **2017**, *488*, 373−389.

(6) Zhu, Y.; Zhao, F.; Wang, W.; Li, Y.; Zhang, S.; Lin, Y. Exciton Binding Energy of Non-Fullerene Electron Acceptors. *Adv. Energy Sustainability Res.* **2022**, *3*, 2100184.

(7) Seo, J. H.; Jin, Y.; Brzezinski, J. Z.; Walker, B.; Nguyen, T. Q. Exciton Binding Energies in Conjugated Polyelectrolyte Films. *ChemPhysChem* **2009**, *10*, 1023−1027.

(8) D'Innocenzo, V.; Grancini, G.; Alcocer, M. J.; Kandada, A. R.; Stranks, S. D.; Lee, M. M.; Lanzani, G.; Snaith, H. J.; Petrozza, A. Excitons versus Free Charges in Organo-lead Tri-halide Perovskites. *Nat. Commun.* **2014**, *5*, 3586.

(9) Alvarado, S. F.; Seidler, P. F.; Lidzey, D. G.; Bradley, D. D. C. Direct Determination of The Exciton Binding Energy of Conjugated Polymers Using A Scanning Tunneling Microscope. *Phys. Rev. Lett.* **1998**, *81*, 1082−1085.

(10) Yang, Y.; Yang, M.; Li, Z.; Crisp, R.; Zhu, K.; Beard, M. C. Comparison of Recombination Dynamics in $CH_3NH_3PbBr_3$ and $CH_3NH_3PbI_3$ Perovskite Films: Influence of Exciton Binding Energy. *J. Phys. Chem. Lett.* **2015**, *6*, 4688−4692.

(11) Miyata, A.; Mitioglu, A.; Plochocka, P.; Portugall, O.; Wang, J. T.-W.; Stranks, S. D.; Snaith, H. J.; Nicholas, R. J. Direct Measurement of The Exciton Binding Energy And Effective Masses for Charge Carriers in Organic−inorganic Tri-halide Perovskites. *Nat. Phys.* **2015**, *11*, 582−587.

(12) Knupfer, M. Exciton Binding Energies in Organic Semiconductors. *Appl. Phys. A: Mater. Sci. Process.* **2003**, *77*, 623−626.

(13) Wang, X.; Huo, D.; Wang, X.; Li, M.; Wang, Y.; Wan, Y. Hot Carrier Dynamics and Charge Trapping in Surface Passivated beta-CsPbI3 Inorganic Perovskite. *J. Phys. Chem. Lett.* **2021**, *12* (29), 6907−6913.

(14) Zhu, T.; Wan, Y.; Huang, L. Direct Imaging of Frenkel Exciton Transport by Ultrafast Microscopy. *Acc. Chem. Res.* **2017**, *50*, 1725−1733.

(15) Karuthedath, S.; Gorenflot, J.; Firdaus, Y.; Chaturvedi, N.; De Castro, C. S. P.; Harrison, G. T.; Khan, J. I.; Markina, A.; Balawi, A. H.; Peña, T. A. D.; et al. Intrinsic Efficiency Limits in Low-Bandgap Non-Fullerene Acceptor Organic Solar Cells. *Nat. Mater.* **2021**, *20*, 378−384.

(16) Kaake, L. G.; Jasieniak, J. J.; Bakus, R. C., 2nd; Welch, G. C.; Moses, D.; Bazan, G. C.; Heeger, A. J. Photoinduced Charge Generation in A Molecular Bulk Heterojunction Material. *J. Am. Chem. Soc.* **2012**, *134*, 19828−19838.

(17) Zhang, G.; Zhao, J.; Chow, P. C. Y.; Jiang, K.; Zhang, J.; Zhu, Z.; Zhang, J.; Huang, F.; Yan, H. Nonfullerene Acceptor Molecules for Bulk Heterojunction Organic Solar Cells. *Chem. Rev.* **2018**, *118*, 3447−3507.

(18) Ward, A. J.; Ruseckas, A.; Kareem, M. M.; Ebenhoch, B.; Serrano, L. A.; Al-Eid, M.; Fitzpatrick, B.; Rotello, V. M.; Cooke, G.; Samuel, I. D. The Impact of Driving Force on Electron Transfer Rates in Photovoltaic Donor-Acceptor Blends. *Adv. Mater.* **2015**, *27*, 2496−2500.

(19) Qian, D.; Zheng, Z.; Yao, H.; Tress, W.; Hopper, T. R.; Chen, S.; Li, S.; Liu, J.; Chen, S.; Zhang, J.; et al. Design Rules for Minimizing Voltage Losses in High-Efficiency Organic Solar Cells. *Nat. Mater.* **2018**, *17*, 703−709.

(20) Menke, S. M.; Ran, N. A.; Bazan, G. C.; Friend, R. H. Understanding Energy Loss in Organic Solar Cells: Toward a New Efficiency Regime. *Joule* **2018**, *2*, 25−35.
(21) Menke, S. M.; Cheminal, A.; Conaghan, P.; Ran, N. A.; Greehnam, N. C.; Bazan, G. C.; Nguyen, T. Q.; Rao, A.; Friend, R. H. Order Enables Efficient Electron-hole Separation at An Organic Heterojunction with A Small Energy Loss. *Nat. Commun.* **2018**, *9*, 277.
(22) Sun, R.; Wu, Y.; Yang, X.; Gao, Y.; Chen, Z.; Li, K.; Qiao, J.; Wang, T.; Guo, J.; Liu, C.; et al. Single-Junction Organic Solar Cells with 19.17% Efficiency Enabled by Introducing One Asymmetric Guest Acceptor. *Adv. Mater.* **2022**, *34*, e2110147.
(23) He, D.; Zhao, F.; Wang, C.; Lin, Y. Non-Radiative Recombination Energy Losses in Non-Fullerene Organic Solar Cells. *Adv. Funct. Mater.* **2022**, *32*, 2111855.
(24) Xing, Z.; Meng, X.; Sun, R.; Hu, T.; Huang, Z.; Min, J.; Hu, X.; Chen, Y. An Effective Method for Recovering Nonradiative Recombination Loss in Scalable Organic Solar Cells. *Adv. Funct. Mater.* **2020**, *30*, 2000417.
(25) Leblebici, S. Y.; Chen, T. L.; Olalde-Velasco, P.; Yang, W.; Ma, B. Reducing Exciton Binding Energy by Increasing Thin Film Permittivity: An Effective Approach To Enhance Exciton Separation Efficiency in Organic Solar Cells. *ACS Appl. Mater. Interfaces* **2013**, *5* (20), 10105−10110.
(26) Zhu, L.; Zhang, J.; Guo, Y.; Yang, C.; Yi, Y.; Wei, Z. Small Exciton Binding Energies Enabling Direct Charge Photogeneration Towards Low-Driving-Force Organic Solar Cells. *Angew. Chem., Int. Ed.* **2021**, *60*, 15348−15353.
(27) Leenaers, P. J.; Maufort, A.; Wienk, M. M.; Janssen, R. A. J. Impact of pi-Conjugated Linkers on the Effective Exciton Binding Energy of Diketopyrrolopyrrole-Dithienopyrrole Copolymers. *J. Phys. Chem. C Nanomater Interfaces* **2020**, *124*, 27403−27412.
(28) Yuan, J.; Zhang, Y.; Zhou, L.; Zhang, G.; Yip, H.-L.; Lau, T.-K.; Lu, X.; Zhu, C.; Peng, H.; Johnson, P. A.; et al. Single-Junction Organic Solar Cell with over 15% Efficiency Using Fused-Ring Acceptor with Electron-Deficient Core. *Joule* **2019**, *3*, 1140−1151.
(29) Zhong, Y.; Causa', M.; Moore, G. J.; Krauspe, P.; Xiao, B.; Gunther, F.; Kublitski, J.; Shivhare, R.; Benduhn, J.; BarOr, E.; et al. Sub-Picosecond Charge-Transfer at Near-Zero Driving Force in Polymer:Non-fullerene Acceptor Blends And Bilayers. *Nat. Commun.* **2020**, *11*, 833.
(30) Sun, C.; Qin, S.; Wang, R.; Chen, S.; Pan, F.; Qiu, B.; Shang, Z.; Meng, L.; Zhang, C.; Xiao, M.; et al. High Efficiency Polymer Solar Cells with Efficient Hole Transfer at Zero Highest Occupied Molecular Orbital Offset between Methylated Polymer Donor and Brominated Acceptor. *J. Am. Chem. Soc.* **2020**, *142*, 1465−1474.
(31) Lin, Y.; He, Q.; Zhao, F.; Huo, L.; Mai, J.; Lu, X.; Su, C.-J.; Li, T.; Wang, J.; Zhu, J.; et al. A Facile Planar Fused-Ring Electron Acceptor for As-Cast Polymer Solar Cells with 8.71% Efficiency. *J. Am. Chem. Soc.* **2016**, *138*, 2973−2976.
(32) Zhang, Z. G.; Li, Y. Polymerized Small-Molecule Acceptors for High-Performance All-Polymer Solar Cells. *Angew. Chem., Int. Ed.* **2021**, *60*, 4422−4433.
(33) Zhang, Z.-G.; Yang, Y.; Yao, J.; Xue, L.; Chen, S.; Li, X.; Morrison, W.; Yang, C.; Li, Y. Constructing a Strongly Absorbing Low-Bandgap Polymer Acceptor for High-Performance All-Polymer Solar Cells. *Angew. Chem., Int. Ed.* **2017**, *56*, 13503−13507.
(34) Du, J.; Hu, K.; Meng, L.; Angunawela, I.; Zhang, J.; Qin, S.; Liebman-Pelaez, A.; Zhu, C.; Zhang, Z.; Ade, H.; Li, Y. High-Performance All-Polymer Solar Cells: Synthesis of Polymer Acceptor by a Random Ternary Copolymerization Strategy. *Angew. Chem., Int. Ed.* **2020**, *59*, 15181−15185.
(35) Yu, H.; Qi, Z.; Yu, J.; Xiao, Y.; Sun, R.; Luo, Z.; Cheung, A. M. H.; Zhang, J.; Sun, H.; Zhou, W.; et al. Fluorinated End Group Enables High-Performance All-Polymer Solar Cells with Near-Infrared Absorption and Enhanced Device Efficiency over 14%. *Adv. Energy Mater.* **2021**, *11*, 2003171.
(36) Du, J.; Hu, K.; Zhang, J.; Meng, L.; Yue, J.; Angunawela, I.; Yan, H.; Qin, S.; Kong, X.; Zhang, Z.; Guan, B.; Ade, H.; Li, Y. Polymerized Small Molecular Acceptor Based All-polymer Solar Cells with an Efficiency of 16.16% via Tuning Polymer Blend Morphology by Molecular Design. *Nat. Commun.* **2021**, *12*, 5264.
(37) Song, Y.; Liu, X.; Li, Y.; Nguyen, H. H.; Duan, R.; Kubarych, K. J.; Forrest, S. R.; Ogilvie, J. P. Mechanistic Study of Charge Separation in a Nonfullerene Organic Donor-Acceptor Blend Using Multispectral Multidimensional Spectroscopy. *J. Phys. Chem. Lett.* **2021**, *12*, 3410−3416.
(38) Savoie, B. M.; Jackson, N. E.; Chen, L. X.; Marks, T. J.; Ratner, M. A. Mesoscopic Features of Charge Generation in Organic Semiconductors. *Acc. Chem. Res.* **2014**, *47*, 3385−3394.
(39) Kolano, C.; Helbing, J.; Kozinski, M.; Sander, W.; Hamm, P. Watching Hydrogen-bond Dynamics in a Beta-turn by Transient Two-dimensional Infrared Spectroscopy. *Nature* **2006**, *444*, 469−472.
(40) Cahoon, J. F.; Sawyer, K. R.; Schlegel, J. P.; Harris, C. B. Determining Transition-state Geometries in Liquids Using 2D-IR. *Science* **2008**, *319*, 1820−1823.
(41) Lei, Y.; Dai, W.; Guan, J.; Guo, S.; Ren, F.; Zhou, Y.; Shi, J.; Tong, B.; Cai, Z.; Zheng, J.; Dong, Y. Wide-Range Color-Tunable Organic Phosphorescence Materials for Printable and Writable Security Inks. *Angew. Chem., Int. Ed. Engl.* **2020**, *59*, 16054−16060.
(42) Guan, J.; Wei, R.; Prlj, A.; Peng, J.; Lin, K. H.; Liu, J.; Han, H.; Corminboeuf, C.; Zhao, D.; Yu, Z.; Zheng, J. Direct Observation of Aggregation-Induced Emission Mechanism. *Angew. Chem., Int. Ed.* **2020**, *59*, 14903−14909.
(43) Khalil, M.; Demirdoven, N.; Tokmakoff, A. Vibrational coherence transfer characterized with Fourier-transform 2D IR spectroscopy. *J. Chem. Phys.* **2004**, *121*, 362−373.
(44) Naraharisetty, S. R. G.; Kasyanenko, V. M.; Rubtsov, I. V. Bond Connectivity Measured via Relaxation-assisted Two-dimensional Infrared Spectroscopy. *J. Chem. Phys.* **2008**, *128*, 104502.
(45) Wang, J. P.; Chen, J. X.; Hochstrasser, R. M. Local Structure of Beta-hairpin Isotopomers by FTIR, 2D IR, and ab initio Theory. *J. Phys. Chem. B* **2006**, *110*, 7545−7555.
(46) Mukherjee, P.; Kass, I.; Arkin, I.; Zanni, M. T. Picosecond Dynamics of A Membrane Protein Revealed by 2D IR. *Proc. Natl. Acad. Sci. U.S.A.* **2006**, *103*, 3528−3533.
(47) Maekawa, H.; Formaggio, F.; Toniolo, C.; Ge, N. H. Onset of 3(10)-helical Secondary Structure in aib Oligopeptides Probed by Coherent 2D IR Spectroscopy. *J. Am. Chem. Soc.* **2008**, *130*, 6556−6566.
(48) Mak, K. F.; Lee, C.; Hone, J.; Shan, J.; Heinz, T. F. Atomically Thin MoS2: A New Direct-gap Semiconductor. *Phys. Rev. Lett.* **2010**, *105*, 136805.
(49) Ye, Z.; Cao, T.; O'Brien, K.; Zhu, H.; Yin, X.; Wang, Y.; Louie, S. G.; Zhang, X. Probing Excitonic Dark States in Single-layer Tungsten Disulphide. *Nature* **2014**, *513*, 214−218.
(50) Chen, H. L.; et al. Ultrafast Formation of Interlayer Hot Excitons in Atomically Thin MoS_2/WS_2 Heterostructures. *Nat. Commun.* **2016**, *7*, 12512−12519.
(51) Barbour, L. W.; Hegadorn, M.; Asbury, J. B. Watching Electrons Move in Real Time: Ultrafast Infrared Spectroscopy of A Polymer Blend Photovoltaic Material. *J. Am. Chem. Soc.* **2007**, *129*, 15884−15894.
(52) Barbour, L. W.; Hegadorn, M.; Asbury, J. B. Microscopic Inhomogeneity and Ultrafast Orientational Motion in An Organic Photovoltaic Bulk Heterojunction Thin Film Studied with 2D IR Vibrational Spectroscopy. *J. Phys. Chem. B* **2006**, *110*, 24281−24286.
(53) Iyer, V.; Segovia, M.; Wang, Y.; Wu, W.; Ye, P.; Xu, X. Infrared Ultrafast Spectroscopy of Solution-Grown Thin Film Tellurium. *Phys. Rev. B* **2019**, *100*, 075436.
(54) Osterbacka, R.; An, C. P.; Jiang, X. M.; Vardeny, Z. V. Two-Dimensional Electronic Excitations in Self-assembled Conjugated Polymer Nanocrystals. *Science* **2000**, *287*, 839−842.
(55) Sheng, C. X.; Kim, K. H.; Tong, M.; Yang, C.; Kang, H.; Park, Y. W.; Vardeny, Z. V. Ultrafast Transient Spectroscopy of Trans-Polyacetylene in the Midinfrared Spectral Range. *Phys. Rev. Lett.* **2020**, *124*, 017401.

https://doi.org/10.1021/acs.jpclett.2c02337
J. Phys. Chem. Lett. 2022, 13, 8816−8824

(56) Tamaki, Y.; Furube, A.; Katoh, R.; Murai, M.; Hara, K.; Arakawa, H.; Tachiya, M. Trapping Dynamics of Electrons And Holes in A Nanocrystalline Tio2 Film Revealed by Femtosecond Visible/near-Infrared Transient Absorption Spectroscopy. *Comptes Rendus Chimie* **2006**, *9*, 268−274.
(57) Pensack, R. D.; Asbury, J. B. Barrierless Free Carrier Formation in An Organic Photovoltaic Material Measured with Ultrafast Vibrational Spectroscopy. *J. Am. Chem. Soc.* **2009**, *131*, 15986−15987.
(58) He, X.; Zhu, G.; Yang, J.; Chang, H.; Meng, Q.; Zhao, H.; Zhou, X.; Yue, S.; Wang, Z.; Shi, J.; et al. Photogenerated Intrinsic Free Carriers in Small-molecule Organic Semiconductors Visualized by Ultrafast Spectroscopy. *Sci. Rep.* **2015**, *5*, 17076.
(59) Guo, Z.; Manser, J. S.; Wan, Y.; Kamat, P. V.; Huang, L. Spatial And Temporal Imaging of Long-range Charge Transport in Perovskite Thin Films by Ultrafast Microscopy. *Nat. Commun.* **2015**, *6*, 7471−7479.
(60) Perdigon-Toro, L.; Zhang, H.; Markina, A.; Yuan, J.; Hosseini, S. M.; Wolff, C. M.; Zuo, G.; Stolterfoht, M.; Zou, Y.; Gao, F.; et al. Barrierless Free Charge Generation in the High-Performance PM6:Y6 Bulk Heterojunction Non-Fullerene Solar Cell. *Adv. Mater.* **2020**, *32*, 1906763.
(61) Zahn, D. R. T.; Gavrila, G. N.; Gorgoi, M. The Transport Gap of Organic Semiconductors Studied Using The Combination of Direct And Inverse Photoemission. *Chem. Phys.* **2006**, *325*, 99−112.
(62) Park, S.; Jeong, J.; Hyun, G.; Kim, M.; Lee, H.; Yi, Y. The Origin Of High PCE in PTB7 Based Photovoltaics: Proper Charge Neutrality Level And Free Energy of Charge Separation at PTB7/PC71BM Interface. *Sci. Rep.* **2016**, *6*, 35262.
(63) Yoshida, H. Principle And Application of Low Energy Inverse Photoemission Spectroscopy: A New Method for Measuring Unoccupied States of Organic Semiconductors. *J. Electron Spectrosc. Relat. Phenom.* **2015**, *204*, 116−124.
(64) Yuan, J.; Zhang, Y.; Zhou, L.; Zhang, C.; Lau, T. K.; Zhang, G.; Lu, X.; Yip, H. L.; So, S. K.; Beaupre, S.; et al. Fused Benzothiadiazole: A Building Block for n-Type Organic Acceptor to Achieve High-Performance Organic Solar Cells. *Adv. Mater.* **2019**, *31*, 1807577.
(65) Luo, Z.; Sun, R.; Zhong, C.; Liu, T.; Zhang, G.; Zou, Y.; Jiao, X.; Min, J.; Yang, C. Altering Alkyl-chains Branching Positions for Boosting The Performance of Small-Molecule Acceptors for Highly Efficient Nonfullerene Organic Solar Cells. *Sci. China Chem.* **2020**, *63*, 361−369.
(66) Luo, Z.; Liu, T.; Ma, R.; Xiao, Y.; Zhan, L.; Zhang, G.; Sun, H.; Ni, F.; Chai, G.; Wang, J.; et al. Precisely Controlling the Position of Bromine on the End Group Enables Well-Regular Polymer Acceptors for All-Polymer Solar Cells with Efficiencies over 15. *Adv. Mater.* **2020**, *32*, 2005942.
(67) Wang, W.; Wu, Q.; Sun, R.; Guo, J.; Wu, Y.; Shi, M.; Yang, W.; Li, H.; Min, J. Controlling Molecular Mass of Low-Band-Gap Polymer Acceptors for High-Performance All-Polymer Solar Cells. *Joule* **2020**, *4*, 1070−1086.
(68) Kraner, S.; Scholz, R.; Plasser, F.; Koerner, C.; Leo, K. Exciton Size And Binding Energy Limitations in One-dimensional Organic Materials. *J. Chem. Phys.* **2015**, *143*, 244905.
(69) Kraner, S.; Prampolini, G.; Cuniberti, G. Exciton Binding Energy in Molecular Triads. *J. Phys. Chem. C* **2017**, *121*, 17088−17095.

https://doi.org/10.1021/acs.jpclett.2c02337
J. Phys. Chem. Lett. 2022, 13, 8816−8824